

**Behavior of an Infinitesimal-Variable-Mass Body in CR3BP; the Primaries are Finite Straight Segments**

Abdullah A. Ansari<sup>1</sup>, Rabah Kellil<sup>2</sup>, Ziyad A. Alhussain<sup>3</sup>

<sup>1,3</sup> Department of Mathematics, University of Majmaah, Saudi Arabia.

<sup>2</sup> Department of Mathematics, University of Monastir, Tunisia.

Email: a.ansari@mu.edu.sa<sup>1</sup>, kellilrabah@yahoo.fr<sup>2</sup>, z.alhussain@mu.edu.sa<sup>3</sup>

Received: 29 May, 2018 / Accepted: 21 December, 2018 / Published online: 05 March, 2019

**Abstract.** In this paper, we deal with the motion of the variable infinitesimal body having a variable mass in CR3BP, when the primaries are assumed to be finite straight segments. We also assume that the primaries are placed in a straight line and move in circular orbits. These orbits are assumed to be around the common center of mass of the primaries and which we take as origin of the coordinates system. The third body is moving under the gravitational forces of the primaries but it does not influence their behavior. We first determine the equations of motion of the infinitesimal body and then the Jacobi-Integral constant. We study numerically the equilibrium points, regions of motion, zero-velocity surfaces with projection, surfaces with variation of Jacobi constant, Poincaré surface of sections and basins of attraction by using Mathematica software. Finally, we examine the stability of the equilibrium points.

**AMS (MOS) Subject Classification Codes:** 70F15; 85A20; 70F05

**Key Words:** R3BP; Finite straight segment; Variable mass; Zero-velocity curves; Poincaré surface of sections; Basins of Attraction.

## 1. INTRODUCTION

The  $n$ -body problem, during the few last decades, attracted many celestial mechanics researchers. In particular, the 3-body and 4-body problems have taken a large part of these researches. They have been studied for different configurations. Some of them have been focused on the shape of the primaries and others on different perturbations introduced on a part or on whole system. Among these perturbations, we can cite the resonance effect, variation of mass on primaries and/or on the infinitesimal body, coriolis and centrifugal forces or Poynting-Robertson effects. System subjected to drag or solar radiation as well as albedo effects have also been intensively studied.

In the present study, by the expression "CR3BP", we mean a system of three bodies, two will be called "the primaries", and the third, will be called "the infinitesimal body". In this configuration, we often suppose that the primaries affect the behavior of the third body, assumed to have no effect on the motion or on the behavior of the primaries.

To recall the history of the  $n$ -body problem, let us cite some remarkable works that inspired the present investigation. [15] investigated many periodical orbits and bifurcations around a massive straight segment. [16] studied the non-linear stability of the four equilibrium points in the gravitational field of a finite straight segment. [8] proved that any truncation of the expansion of the potential does not admit meromorphic integrals other than the Hamiltonian itself. [9] performed a simple model to determine chaotic motions around asteroids which are considered as a rotating finite straight segment. [10] studied the stability and locations of the Lagrangian equilibrium points in the CR3BP, under the assumption that both the primaries are finite straight segments.

Many other researchers studied the CR3BP with variable masses. We can cite [11], [14], [17], [12], [18], [19], [20], [21], [13], [22], [1]. On the other hand, many other researchers studied the basins of attraction in the restricted problem as [2], [3], [4], [5], [6], [7], [23], [24], [25], etc...

As a contribution to these questions, we investigate the behavior of the infinitesimal body in CR3BP, where we suppose that its mass varies and where the primaries are assumed to be straight segments. We start our paper by deriving the equations of motion from Newton's law and the momentum equation, and then we determine the time variation of Jacobi constant. In the next section, we perform all the aspects of the numerical analysis related to our question: equilibrium points, regions of motion, zero-velocity surfaces with projection, surfaces with variation of Jacobi constant, Poincaré surface of sections and Newton-Raphson basins of attraction. After the above study, we examine the stability of the equilibrium points. Finally, we interpret the principal results of our problem.

Our principal motivation is that, this problem has many applications in the control of space stations that can be assimilated to straight segments and can serve for a model of precise further investigations.

## 2. STATEMENT OF THE PROBLEM AND EQUATIONS OF MOTION

Let  $m_1$  and  $m_2$  be the masses ( $m_1 > m_2$ ) of two bodies supposed to be finite segments denoted by  $AB$  and  $CD$  with lengths  $2L_1$  and  $2L_2$  respectively. The finite segments  $AB$  and  $CD$  are placed on the  $x$ -axis and are moving around their common center of mass taken as the origin  $O$ . The line orthogonal to the  $x$ -axis, passing through  $O$  is supposed to be the  $y$ -axis. The distances of the third infinitesimal-variable-mass body; mass of which is denoted by  $m(t)$ ; from  $A, B, C$ , and  $D$  are  $S_1, S_2, R_1$  and  $R_2$  respectively. The infinitesimal-variable-mass body denoted by  $m(t)$  is moving under the influence of these two primaries but does not have any influence on them. We will be concerned by the synodic coordinate system; which coincides initially with the inertial coordinate system, and revolving with angular velocity  $\omega$ . Let the coordinates of  $m_1, m_2$  and  $m(t)$  in the rotating frame be  $(x_1, 0), (x_2, 0)$  and  $(x, y)$  respectively (Fig. 1). The total gravitational potential  $V$  of these straight segments evaluated at the point  $P$  is  $V = V_1 + V_2$ , Where  $V_1, V_2$  are respectively the potential of the segment  $AB$  and the potential of the segment  $CD$ , explicitly given by (see [10])

$$\begin{cases} V_1 = -\frac{Gm_1m(t)}{2L_1} \log\left\{\frac{S_1+S_2+2L_1}{S_1+S_2-2L_1}\right\} \\ V_2 = -\frac{Gm_2m(t)}{2L_2} \log\left\{\frac{R_1+R_2+2L_2}{R_1+R_2-2L_2}\right\} \end{cases}$$

Assume that the sum of masses of the primaries is unity, i.e.  $m_1 + m_2 = 1$ , the distances between the center of mass and the primaries are unity, i.e.  $EF = R = 1$ . The unit of time is chosen such that the gravitational constant  $G$  becomes unity. Taking  $\frac{m_2}{(m_1+m_2)} = \mu$ , then  $m_2 = \mu$ , and  $m_1 = 1 - \mu$ . Therefore, the dimensionless coordinates of the points  $E$  and  $F$  will be  $(\mu, 0)$  and  $(\mu - 1, 0)$  respectively.

Following the procedure given by [1], we can write the equations of motion of the infinitesimal-variable-mass in the rotating coordinate system when the variation of mass is non-isotropic with zero momentum as

$$\begin{cases} \frac{\dot{m}(t)}{m(t)}(\dot{x} - \omega y) + (\ddot{x} - 2\omega \dot{y}) = \frac{\partial \Omega}{\partial x} \\ \frac{\dot{m}(t)}{m(t)}(\dot{y} + \omega x) + (\ddot{y} + 2\omega \dot{x}) = \frac{\partial \Omega}{\partial y}. \end{cases} \quad (2.1)$$

where

$$\Omega = \frac{\omega^2}{2}(x^2 + y^2) + \frac{(1-\mu)}{2l_1} \log\left\{\frac{S_1+S_2+2l_1}{S_1+S_2-2l_1}\right\} + \frac{\mu}{2l_2} \log\left\{\frac{R_1+R_2+2l_2}{R_1+R_2-2l_2}\right\},$$

$$S_1^2 = (x - (\mu + l_1))^2 + y^2, \quad S_2^2 = (x - (\mu - l_1))^2 + y^2,$$

$$R_1^2 = (x - (\mu - 1 + l_2))^2 + y^2, \quad R_2^2 = (x - (\mu - 1 - l_2))^2 + y^2,$$

$$l_1 = \frac{L_1}{R}, \quad l_2 = \frac{L_2}{R}, \quad \text{and } \omega^2 = (1 + l_1^2 + l_2^2). \quad [10]$$

Due to variation of mass of infinitesimal body, we use Jeans' law  $\frac{dm}{dt} = -\lambda_1 m^n$ , where  $\lambda_1$  is a variation constant and the value of exponent  $n$  is in between  $0.4 \leq n \leq 4.4$  for stars and it is unity for rockets. Notice, therefore, that the mass of the rocket varies exponentially as  $m = m_0 e^{-\lambda_1 t}$ .

Now, we use space-time transformation taking into account the transformations given in [17] by:

$$x = \varepsilon^{-1/2} \xi, \quad y = \varepsilon^{-1/2} \eta, \quad dt = d\tau, \quad S_i = \varepsilon^{-1/2} s_i, \quad R_i = \varepsilon^{-1/2} r_i, \quad (i = 1, 2). \quad \text{where } \varepsilon = \frac{m}{m_0}.$$

And hence,

$$\dot{x} = \varepsilon^{-1/2}(\xi' + \frac{\lambda_1}{2}\xi), \quad \dot{y} = \varepsilon^{-1/2}(\eta' + \frac{\lambda_1}{2}\eta), \quad \ddot{x} = \varepsilon^{-1/2}(\xi'' + \lambda_1 \xi' + \frac{\lambda_1^2}{4}\xi), \quad \ddot{y} = \varepsilon^{-1/2}(\eta'' + \lambda_1 \eta' + \frac{\lambda_1^2}{4}\eta). \quad \text{where, dot } (\cdot) \text{ and prime } (') \text{ represent the derivative w.r. to } t \text{ and } \tau \text{ respectively.}$$

Using these transformation, equations of motion (2.1) become

$$\begin{cases} \xi'' - 2\omega \eta' = \frac{\partial \psi}{\partial \xi} \\ \eta'' + 2\omega \xi' = \frac{\partial \psi}{\partial \eta}. \end{cases} \quad (2.2)$$

where

$$\psi = \left(\frac{\omega^2}{2} + \frac{\lambda_1^2}{8}\right)(\xi^2 + \eta^2) + \frac{(1-\mu)\varepsilon^{3/2}}{2l_1} \log\left\{\frac{s_1+s_2+2l_1\varepsilon^{1/2}}{s_1+s_2-2l_1\varepsilon^{1/2}}\right\} + \frac{\mu\varepsilon^{3/2}}{2l_2} \log\left\{\frac{r_1+r_2+2l_2\varepsilon^{1/2}}{r_1+r_2-2l_2\varepsilon^{1/2}}\right\}.$$

$$s_1^2 = (\xi - \varepsilon^{1/2}(\mu + l_1))^2 + \eta^2, s_2^2 = (\xi - \varepsilon^{1/2}(\mu - l_1))^2 + \eta^2,$$

$$r_1^2 = (\xi - \varepsilon^{1/2}(\mu - 1 + l_2))^2 + \eta^2, r_2^2 = (\xi - \varepsilon^{1/2}(\mu - 1 - l_2))^2 + \eta^2,$$

The Jacobi-Integral can also be written as

$$\xi'^2 + \eta'^2 = 2\psi - C - 2 \int_{\tau_0}^{\tau} \frac{\partial \psi}{\partial \tau} d\tau. \quad (2.3)$$

where, C is the Jacobi-integral constant.

### 3. NUMERICAL SECTION

In this section, we are concerned by the numerical study of the equilibrium points, regions of motion, zero-velocity surfaces with projection, surfaces of motion of infinitesimal body with the variation of Jacobi-constant, Poincaré surfaces of section and basins of attraction that we draw for  $\mu = 0.03$  and  $\varepsilon = 0.1$ .

**3.1. Equilibrium points.** The equilibrium points are the solutions of the right hand sides of the system (2.2). When we replace all the derivatives by zero in the left hand side of the system (2.2), we get  $\frac{\partial \psi}{\partial \xi} = 0, \frac{\partial \psi}{\partial \eta} = 0$ . Using Mathematica software, we plot the locations of the equilibrium points for different values of the variation constant  $\lambda_1$  ( $= 0.2$ (green),  $0.6$  (red),  $1$  (blue)). We find that the system has at most five equilibrium points ( $L_1, L_2, L_3, L_4, L_5$ ). Among these equilibrium points, three are collinear and two are non-linear. From the figures obtained, we observe that, when we increase the values of variation constant  $\lambda_1$ , the equilibrium points are moving towards the origin (*Fig.2a*). This phenomenon can be observed clearly from figures (2b, 2c) which are the zoomed part of Fig.(2a).

**3.2. Regions of motion.** Following the procedure given by [1], we study the dynamical behavior of the infinitesimal body by drawing its regions of motion in accordance with the values of Jacobi-constant. We plot its regions of motion and find that it can not move in the shaded regions. As the values of the Jacobi-constant decrease, the shaded regions decrease. In the figures 3a, 3b, 3c, 3d, light blue color represents the forbidden regions and infinitesimal body can move only in the white regions. In the Fig. 3(a), at the Jacobi-constant  $C_{L_1} = 0.1979159$ , the infinitesimal body can move in the circular region near  $L_1$  and this point represents a limiting point. It can also move in circular white region near  $L_2$ . In the Fig. 3(b), at the Jacobi-constant  $C_{L_2} = 0.1655264$ , the infinitesimal body can move in the circular region near  $L_2$  and  $L_2$  is the limiting point for this motion. In the Fig. 3(c), at the Jacobi-constant  $C_{L_3} = 0.1289780$ ,  $L_3$  is the limiting point and the infinitesimal body can move in the white regions except the shaded regions near  $L_4$  and  $L_5$ . In the Fig. 3(d), at the Jacobi-constant  $C_{L_{4,5}} = 0.1190430$ , there is no limiting point, the infinitesimal body can move freely any-where in the white region except the shaded regions near  $L_4$  and  $L_5$  look like two icebergs.

**3.3. Zero-velocity surfaces with projections.** In this subsection, we draw the projections of the zero-velocity surfaces in the  $(\xi, \eta)$ -plane for the CR3BP, when the primaries are finite-straight segments and the infinitesimal body have a variable mass in accordance with Jean's law. The motion is possible inside the shaded regions. We observe that the forbidden region decreases when the value of Jacobian constant decreases (Fig. 4a, 4b, 4c, 4d).

**3.4. Surfaces with variation of Jacobi-constant.** In this part, we study the surfaces of motion of the infinitesimal body with the variation of the Jacobi-constant  $C$ . We notice that the motion is possible only in the shaded region which appeared as a bowl. The circumference of the bowl increases when the value of the Jacobi-constant  $C$  increases (Fig. 5).

**3.5. Poincaré surfaces of section.** The Poincaré surfaces of section are drawn for the different values of the variation constant ( $\lambda_1 = 0.2$  (Green), 0.6 (Red), 1 (Blue)) in two different phase spaces ( $\xi - \xi'$ ) Fig 6(a) and ( $\eta - \eta'$ ) Fig6(b). From the Figure 6(a), we observe that, when we increase the value of  $\lambda_1$ , the surfaces are shrinking for  $\xi \in [0.05, 0.17]$  and expanding outside this interval. From the Figure 6(b), we observe that for  $\eta' \geq 0.1$  and  $\lambda_1 \in [0.6, 1]$ , the surfaces are close to each other.

**3.6. Basins of Attraction.** Here, we draw the Newton-Raphson basins of attraction for the CR3BP, where the primaries are taken as finite-straight segments and the infinitesimal body has variable mass according to the Jean's law. It is accurate and fast computational tool to evaluate the basins of convergence. The algorithm of our problem is given by:

$$\begin{cases} \xi_{n+1} = \xi_n - \left( \frac{\psi_\xi \psi_{\eta\eta} - \psi_\eta \psi_{\xi\xi}}{\psi_{\xi\xi} \psi_{\eta\eta} - \psi_{\xi\eta} \psi_{\eta\xi}} \right)_{(\xi_n, \eta_n)}, \\ \eta_{n+1} = \eta_n - \left( \frac{\psi_\eta \psi_{\xi\xi} - \psi_\xi \psi_{\eta\eta}}{\psi_{\xi\xi} \psi_{\eta\eta} - \psi_{\xi\eta} \psi_{\eta\xi}} \right)_{(\xi_n, \eta_n)}. \end{cases} \quad (3.4)$$

Where  $\xi_n, \eta_n$  are respectively the values of  $\xi$  and  $\eta$  coordinates of the  $n^{th}$  step of the Newton-Raphson iterative process. If the initial point converges rapidly to one of the attractor then this point  $(\xi, \eta)$  will be the basin of attraction of the root. The process that we propose stops when the successive approximations converge to an equilibrium point that represent an attractor. We use color code to classify the different equilibrium points on the  $(\xi, \eta)$ -plane. In the first case, for  $\lambda_1 = 0.2$  (Fig.7(a)),  $L_1, L_2$  and  $L_3$  represent blue color regions,  $L_4$  represents green color region while  $L_5$  represents yellow color region. The basins of attraction corresponding to all the equilibrium points extend to infinity. In the second case for  $\lambda_1 = 0.6$  (Fig.8(a)),  $L_1, L_2$  and  $L_3$  represent blue color regions,  $L_4$  represents light green color region while  $L_5$  represents light yellow color region. The basins of attraction corresponding to all the equilibrium points extend to infinity. In the third case; for  $\lambda_1 = 1$  (Fig.9(a)),  $L_1, L_2$  and  $L_3$  represent light blue color regions,  $L_4$  represents red color region while  $L_5$  represents green color region. The basins of attraction corresponding to all the equilibrium points extend to infinity. We then get a complete view of the basins structure created by the attractors. It can also be observed in detail in the zoomed part of the figures like Fig.7(b), Fig.8(b), Fig.9(b). We also observe that by increasing the effect of the variation constant  $\lambda_1$ , the basins of attraction shrink. The black points and red points denote the location of the equilibrium points and the primaries respectively.

#### 4. STABILITY OF EQUILIBRIUM POINTS

In this part of the paper, we examine the stability of the equilibrium points in the restricted three-body problem when the primaries are finite-straight-segments and the infinitesimal body has variable mass. If we set  $\xi = \xi_0 + \alpha$ ,  $\eta = \eta_0 + \beta$ , in system (2), we get

the variational equations of system as

$$\begin{cases} \alpha'' - 2\omega\beta' = \alpha\psi_{\xi\xi}^0 + \beta\psi_{\xi\eta}^0 \\ \beta'' + 2\omega\alpha' = \alpha\psi_{\eta\xi}^0 + \beta\psi_{\eta\eta}^0 \end{cases} \quad (4.5)$$

Where  $\alpha$  and  $\beta$  are small displacements from the equilibrium point  $(\xi_0, \eta_0)$  of the infinitesimal body. The superscript zero denotes the value at the equilibrium point.

We can rewrite the system (4.5), in the linear form, as

$$\begin{cases} \alpha' = \alpha_1 \\ \beta' = \beta_1 \\ \alpha'_1 = 2\omega\beta_1 + \alpha\psi_{\xi\xi}^0 + \beta\psi_{\xi\eta}^0 \\ \beta'_1 = -2\omega\alpha_1 + \alpha\psi_{\eta\xi}^0 + \beta\psi_{\eta\eta}^0 \end{cases} \quad (4.6)$$

At  $\lambda_1 = 0$ , the system (4.6) becomes a system with constant mass. For  $\lambda_1 > 0$ , the ordinary method cannot be used to determine the linear stability due to the variation with respect to the time of the distances between the primaries and equilibrium point. Therefore, Meshcherskii space-time inverse transformations will be used.

For the following values,  $x_1 = \varepsilon^{-1/2}\alpha$ ,  $y_1 = \varepsilon^{-1/2}\beta$ ,  $x_2 = \varepsilon^{-1/2}\alpha_1$ ,  $y_2 = \varepsilon^{-1/2}\beta_1$ .

The matrix form of the system (4.6) is as follows:

$$\begin{pmatrix} \frac{dx_1}{d\tau} \\ \frac{dy_1}{d\tau} \\ \frac{dx_2}{d\tau} \\ \frac{dy_2}{d\tau} \end{pmatrix} = A \times \begin{pmatrix} x_1 \\ y_1 \\ x_2 \\ y_2 \end{pmatrix} \quad (4.7)$$

where

$$A = \begin{pmatrix} \frac{\lambda_1}{2} & 0 & 1 & 0 \\ 0 & \frac{\lambda_1}{2} & 0 & 1 \\ (\psi_{\xi\xi})_0 & (\psi_{\xi\eta})_0 & \frac{\lambda_1}{2} & 2\omega \\ (\psi_{\eta\xi})_0 & (\psi_{\eta\eta})_0 & -2\omega & \frac{\lambda_1}{2} \end{pmatrix}$$

The characteristic polynomial of the matrix  $A$  is

$$\begin{aligned} \lambda^4 - 2\lambda_1\lambda^3 + \lambda^2\left(\frac{3\lambda_1^2}{2} + 4\omega^2 - \psi_{\xi\xi} - \psi_{\eta\eta}\right) - \lambda\lambda_1\left(\frac{\lambda_1^2}{2} + 4\omega^2 - \psi_{\xi\xi} - \psi_{\eta\eta}\right) \\ + \frac{1}{16}(\lambda_1^4 - 4\psi_{\xi\xi}\lambda_1^2 - 4\psi_{\eta\eta}\lambda_1^2 + 16\omega^2\lambda_1^2 + 16\psi_{\xi\xi}\psi_{\eta\eta} - 16\psi_{\xi\eta}\psi_{\eta\xi}) \end{aligned} \quad (4.8)$$

So the roots of corresponding characteristic equation are given in the table (1), performed for different values of the variation parameter  $\lambda_1$ . We can observe from the table, that we have at least one positive real parts of the roots (dark black in the table) corresponding to each equilibrium points. From the figure (10), we can also see that there is no bounded region. We can conclude that every equilibrium points are unstable.

## 5. CONCLUSION

We have determined the equations of motion which are different from the classical cases by  $\lambda_1$  and  $\varepsilon$ . In our case the Jacobi integral is different by an integral term. In the numerical section, we found the five equilibrium points which are moving towards the origin when the values of the variation parameter  $\lambda_1$  increases. We also notice that, when we decrease the Jacobi constant, the forbidden region decreases. Assigning the value 0.2 to  $\lambda_1$ , we have drawn the zero-velocity surfaces with projections and the surfaces of motion of the infinitesimal body as a function of the Jacobi constant in  $[0, 0.3]$ . After studying the above parameters, we have been concerned by the Poincaré surfaces of sections, which have been done in two different phase spaces;  $(\xi, \xi')$  and  $(\eta, \eta')$ . We notice that there is an important variation in these surfaces in accordance with the variation of  $\lambda_1$ . Among the questions that have been studied in our paper, the basins of attraction occupied a important part of our investigations. As it has presented we have assigned different colors to attracting unbounded regions. the observation that can be made is that, when we increase the the values of  $\lambda_1$ , the basins of attraction shrink. For the part devoted to stability, we have determined for each equilibrium point, all the characteristic roots. Since we found that among these roots, one at least is a positive real or has positive real part, we conclude that all the equilibrium points are unstable.

## 6. ACKNOWLEDGMENTS

The present work has been accomplished under University of Majmaah Grant 21-1440. We are thankful to the Deanship of Scientific Research of Majmaah University, Kingdom of Saudi Arabia, for providing all other research facilities in the completion of this research work.

## REFERENCES

- [1] E. I. Abouelmagd and A. Mostafa, *Out of plane equilibrium points locations and the forbidden movement regions in the restricted three-body problem with variable mass*, *Astrophys. Space Sci.* **357**, No. 58 (2015).
- [2] A. A. Ansari, *Stability of the equilibrium points in the photogravitational circular restricted four body problem with the effect of perturbations and variable mass*, *Science International Lahore* **28**, (2016a) 859-866.
- [3] A. A. Ansari, *Stability of the equilibrium points in the circular restricted four body problem with oblate primary and variable mass*, *International Journal of Advanced Astronomy* **4**, No. 1 (2016b) 14-19.
- [4] A. A. Ansari, *The Photogravitational Circular Restricted Four-body Problem with Variable Masses*, *Journal of Engineering and Applied Sciences* **3**, No. 2 (2016c) 30-38.
- [5] A. A. Ansari, R. Kellil and Z. Alhussain, *The effect of perturbations on the circular restricted four-body problem with variable masses*, *J. Math. Computer Sci.* **17**, No. 3 (2016d) 365-377.
- [6] A. A. Ansari, *The circular restricted four-body problem with variable masses*, *Nonlinear Sci. Lett. A* **8**, No. 3 (2017a) 303-312.
- [7] A. A. Ansari, *Effect of Albedo on the motion of the infinitesimal body in circular restricted three-body problem with variable masses*, *Italian J. of Pure and Applied Mathematics* **38**, (2017b) 581-600.

- [8] M. Arribas and A. Elipe, *Non-integrability of the motion of a particle around a massive straight segments*, Phys. Lett. A **281**, No. (2-3)(2001) 142-148.
- [9] A. Elipe and M. Lara, *A simple model to determine chaotic motions around asteroids*, Carlos, A. et al eds: The International Meeting of Dynamics in Latin America **25**, (2006) 3-6.
- [10] R. Jain and D. Sinha, *Stability and regions of motion in the restricted three-body problem when both the primaries are finite straight segments*, Astrophys. Space sci. **32**, (2014) 297-305.
- [11] J. H. Jeans, *Astronomy and Cosmogony*, Cambridge University Press, Cambridge 1928.
- [12] H. Lichtenegger, *The dynamics of bodies with variable masses*, Celest. Mech. **34**, (1984) 357-368.
- [13] L. G. Lukyanov, *On the restricted circular conservative three-body problem with variable masses*, Astronomy Letters **35**, No. 5 (2009) 349-359.
- [14] I. V. Meshcherskii, *Works on the Mechanics of Bodies of Variable Mass*, GITTL, Moscow, 1952.
- [15] A. Riaguas, A. Elip and M. Lara, *Periodic orbits around a massive straight segment*, Celest. Mech. Dyn. Astro. **73**, No. (1/4) (1999) 169-178.
- [16] A. Riaguas, A. Elip and T. Lopez-Moratalla, *Non-linear stability of the equilibrium in the gravity of a finite straight segment*, Celest. Mech. Dyn. Astro. **81**, No. 3 (2001) 235-248.
- [17] A. K. Shrivastava and B. Ishwar, *Equations of motion of the restricted problem of three bodies with variable mass*, Celest. Mech. **30**, (1983) 323-328.
- [18] J. Singh and B. Ishwar, *Effect of perturbations on the location of equilibrium points in the restricted problem of three bodies with variable mass*, Celest. Mech. **32**, (1984) 297-305.
- [19] J. Singh and B. Ishwar, *Effect of perturbations on the stability of triangular points in the restricted problem of three bodies with variable mass*, Celest. Mech. **35**, (1985) 201-207.
- [20] J. Singh, *Photogravitational restricted three-body problems with variable mass*, Indian Journal of Pure and Applied Math. **32**, No. 2 (2003) 335-341.
- [21] J. Singh and O. Leke, *Stability of photogravitational restricted three body problem with variable mass*, Astrophys. Space Sci. **326**, No. 2 (2010) 305-314.
- [22] M. J. Zhang, C. Y. Zhao and Y. Q. Xiong, *On the triangular libration points in photo-gravitational restricted three-body problem with variable mass*, Astrophys. Space Sci. **337**, (2012) 107-113, doi 10.1007/s10509-011-0821-8.
- [23] E. E. Zotos, *Investigating the Newton-Raphson basins of attraction in the restricted three-body problem with modified Newtonian gravity*, J. Appl. Math. Comput. (Oct 2016) 1-19.
- [24] E. E. Zotos, *Revealing the basins of convergence in the planar equilateral restricted four body problem*, Astrophys. Space Sci. **362**, No. 2 (2017).
- [25] E. E. Zotos and M. S. Suraj, *Basins of attraction of equilibrium points in the planar circular restricted five-body problem*, Astrophys. Space Sci. **363**, No. 20 (2018).

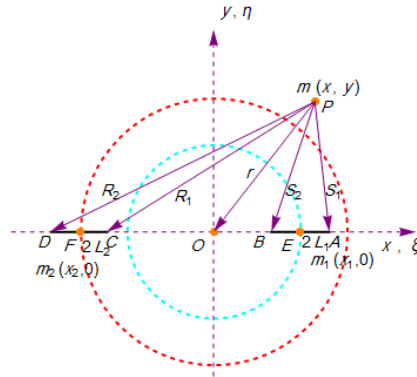


FIGURE 1. Configuration of the problem in CR3BP with the finite straight segment primaries.

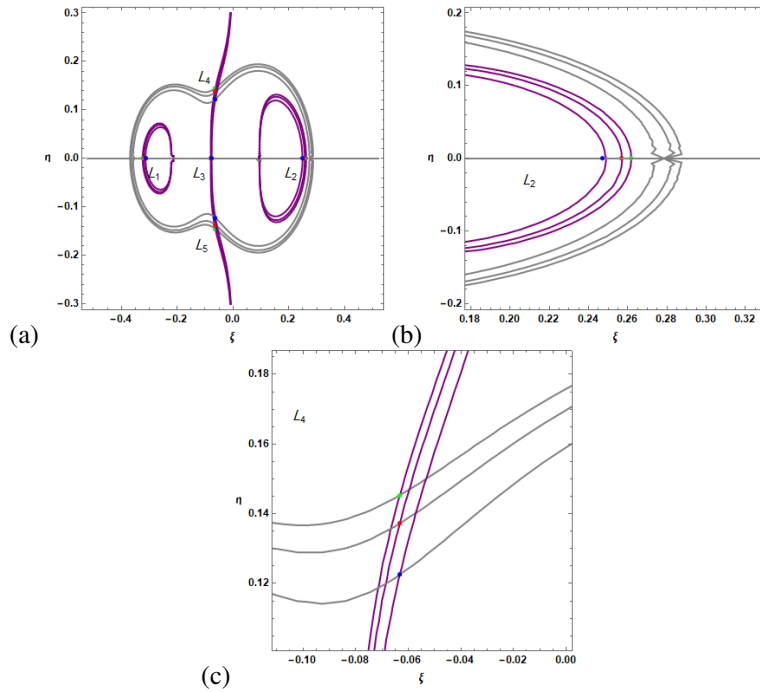


FIGURE 2. (a): Locations of equilibrium points at  $\lambda_1 = 0.2$  (Green),  $0.6$  (Red),  $1$  (Blue). (b, c): The zoomed part of (a) near  $L_2$  and  $L_4$ .

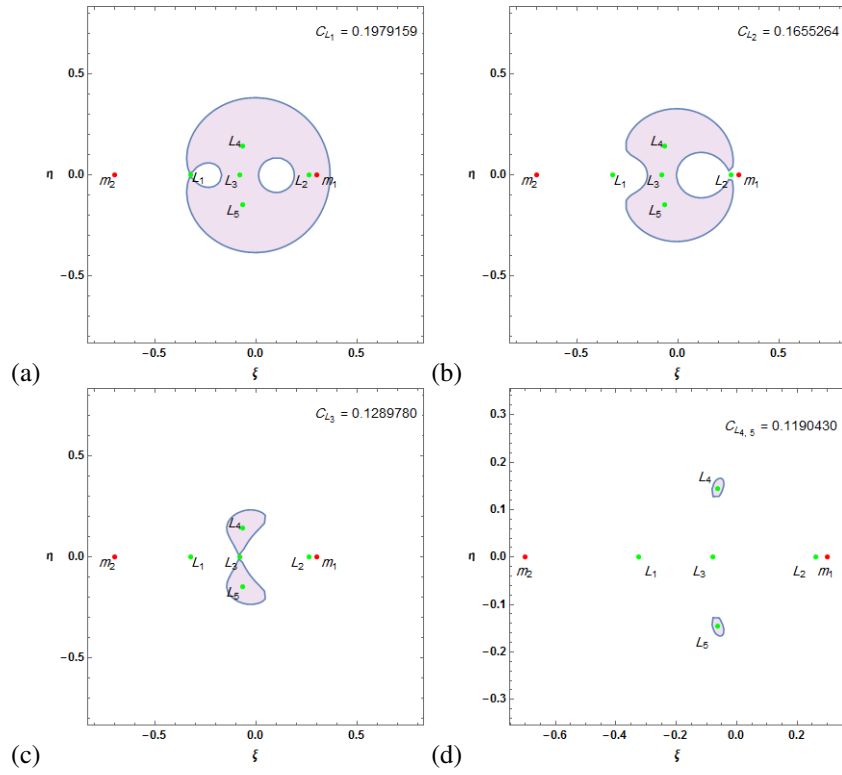


FIGURE 3. Regions of motion at  $\lambda_1 = 0.2$  and various values of Jacobi-constant ( $C_{L_1} = 0.19791599$ (a),  $C_{L_2} = 0.16552647$ (b),  $C_{L_3} = 0.12897801$ (c),  $C_{L_{4,5}} = 0.11904303$ (d)).

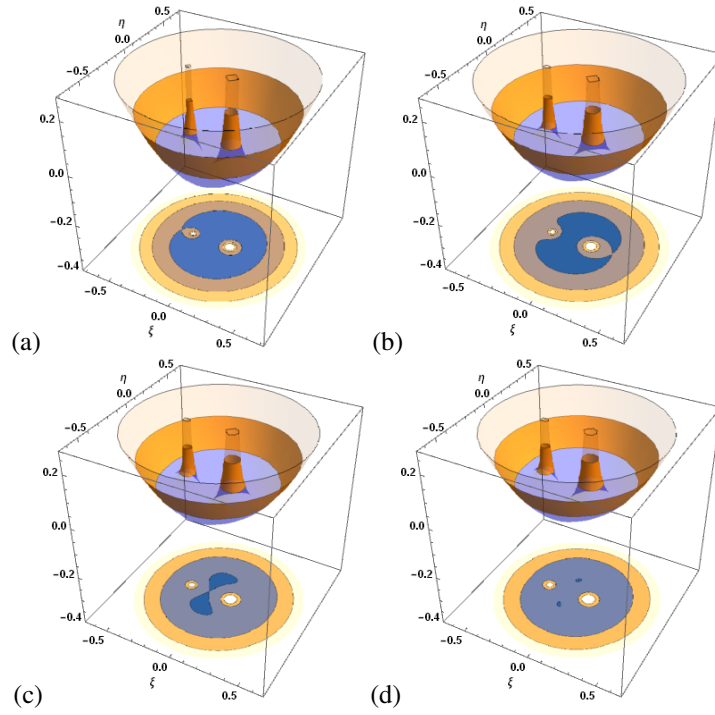


FIGURE 4. Zero-velocity surfaces with projections at ( $C_{L_1} = 0.1979159$ (a),  $C_{L_2} = 0.1655264$ (b),  $C_{L_3} = 0.1289780$ (c),  $C_{L_{4,5}} = 0.1190430$ (d)).

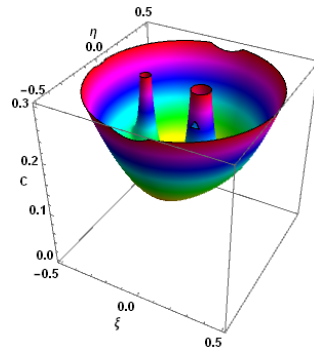


FIGURE 5. The surfaces of motion of the infinitesimal body with the variation of the Jacobi-constant  $C$ .

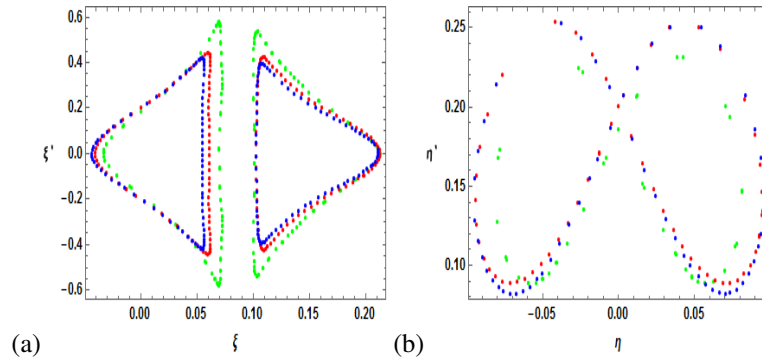


FIGURE 6. Poincaré surfaces of section at different values of variation constant  $\lambda_1$  (at 0.2 (Green), 0.6 (Red), 1 (Blue))

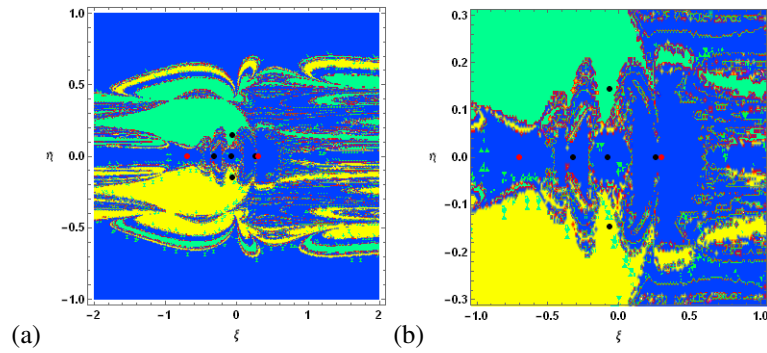


FIGURE 7. (a): Basins of attraction at  $\lambda_1 = 0.2$ , (b): Zoomed part of figure a near the primaries.

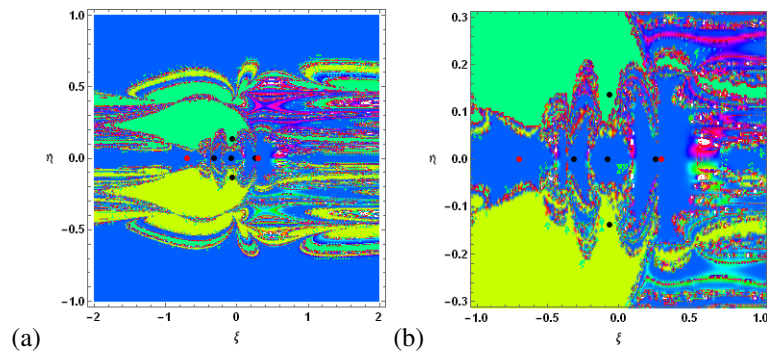


FIGURE 8. (a): Basins of attraction at  $\lambda_1 = 0.6$ , (b): Zoomed part of figure a near the primaries.

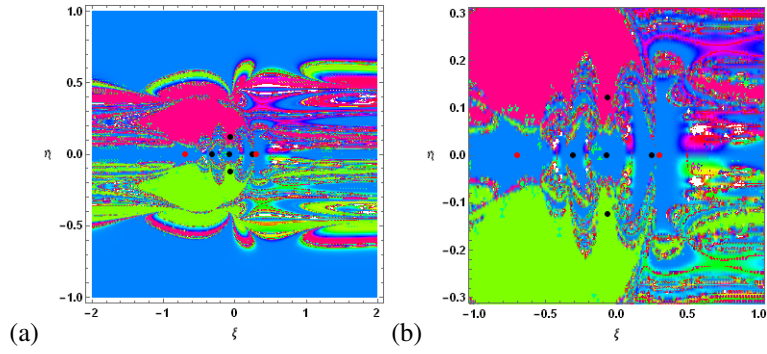


FIGURE 9. (a): Basins of attraction at  $\lambda_1 = 1$ , (b): Zoomed part of figure a near the primaries.

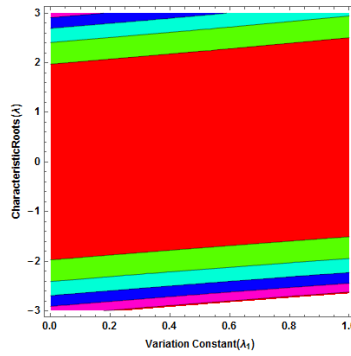


FIGURE 10. Instability regions of the equilibrium points when the primaries are finite-straight-segments and variable-infinitesimal-body

TABLE 1. Values of the Characteristic Roots corresponding to the equilibrium points

Variation constant $\lambda_1$	Equilibrium points	Characteristic Roots
0.2	(0.2617257, 0)	-1.0209887 <b>1.2209887</b> <b>0.1000000</b> - 1.3047240 <i>i</i> <b>0.1000000</b> + 1.3047240 <i>i</i>
	(-0.3236154, 0)	-1.9197919 <b>2.1197919</b> <b>0.1000000</b> - 1.7771877 <i>i</i> <b>0.1000000</b> + 1.7771877 <i>i</i>
	(-0.0796611, 0)	-1.6326886 <b>1.8326886</b> <b>0.1000000</b> - 1.6156634 <i>i</i> <b>0.1000000</b> + 1.6156634 <i>i</i>
	(-0.0632369, 0.1452963)	-0.5703019 - 0.9666205 <i>i</i> -0.5703019 + 0.9666205 <i>i</i> <b>0.7703019</b> - 0.9666205 <i>i</i> <b>0.7703019</b> + 0.9666205 <i>i</i>
	(-0.0632369, -0.1452963)	-0.5703019 - 0.9666205 <i>i</i> -0.5703019 + 0.9666205 <i>i</i> <b>0.7703019</b> - 0.9666205 <i>i</i> <b>0.7703019</b> + 0.9666205 <i>i</i>
	0.6	(0.2567257, 0)
(-0.3183615, 0)		-1.9590414 <b>2.5590414</b> <b>0.2999999</b> - 1.8807850 <i>i</i> <b>0.2999999</b> + 1.8807850 <i>i</i>
(-0.0796611, 0)		-1.4391371 <b>2.0391371</b> <b>0.2999999</b> - 1.5725000 <i>i</i> <b>0.2999999</b> + 1.5725000 <i>i</i>
(-0.0633698, 0.1372963)		-0.4478124 - 0.9617791 <i>i</i> -0.4478124 + 0.9617791 <i>i</i> <b>1.0478124</b> - 0.9617791 <i>i</i> <b>1.0478124</b> + 0.9617791 <i>i</i>
(-0.0633698, -0.1372963)		-0.4478124 - 0.9617791 <i>i</i> -0.4478124 + 0.9617791 <i>i</i> <b>1.0478124</b> - 0.9617791 <i>i</i> <b>1.0478124</b> + 0.9617791 <i>i</i>
1		(0.2472577, 0)
	(-0.3136154, 0)	-2.1884543 <b>2.7884543</b> <b>0.2999999</b> - 2.0221655 <i>i</i> <b>0.2999999</b> + 2.0221655 <i>i</i>
	(-0.0756611, 0)	-1.4453772 <b>2.0453772</b> <b>0.3000000</b> - 1.5760816 <i>i</i> <b>0.3000000</b> + 1.5760816 <i>i</i>
	(-0.0633984, 0.1225296)	-0.4736241 - 0.9403442 <i>i</i> -0.4736241 + 0.9403442 <i>i</i> <b>1.0736241</b> - 0.9403442 <i>i</i> <b>1.0736241</b> + 0.9403442 <i>i</i>
	(-0.0636984, -0.1231529)	-0.4736241 - 0.9403442 <i>i</i> -0.4736241 + 0.9403442 <i>i</i> <b>1.0736241</b> - 0.9403442 <i>i</i> <b>1.0736241</b> + 0.9403442 <i>i</i>